Journal of Nanobiotechnology

RESEARCH

Open Access

Bacterial extracellular biomolecules-derived multimodal manganese nanoparticles control watermelon Fusarium wilt by dysregulating fusaric acid biosynthesis pathway and precise tuning of rhizosphere metabolome

Muhammad Noman[1], Temoor Ahmed[2,3], Mohammad Shafiqul Islam[1,4], Jing Wang[1], Yingying Cai[1], Shuang Liang[5], Zhongna Hao[1], Hayssam M. Ali[6], Haiping Qiu[1], Zhen Zhang[1], Rongyao Chai[1], Yanli Wang[1*], Bin Li[4] and Jiaoyu Wang[1*]

Abstract

Fusarium wilt, caused by *Fusarium oxysporum* f. sp. *niveum* (*Fon*), poses a significant threat to watermelon production globally. Traditional control methods often rely on chemical fungicides, which pose environmental risks and limited long-term efficacy. This study introduces biogenically-synthesized manganese nanoparticles (MnNPs) as a potent antifungal agent for managing Fusarium wilt. MnNPs were synthesized extracellularly using the culture supernatant of *Lysinibacillus sphaericus* NOTE11, a Mn-resistant bacterial strain isolated and characterized in this study. Comprehensive physicochemical analyses confirmed their crystalline structure, spherical morphology, and elemental composition. MnNPs demonstrated potent antifungal activity, significantly inhibiting *Fon* growth, conidiation, and conidial germination in vitro, with 100 µg/mL MnNPs reducing hyphal growth by 21.97% and conidial germination by 80% compared to untreated controls. Disease assays further confirmed that MnNPs significantly reduced Fusarium wilt severity in watermelon (~84%) compared with *Fon*-infected controls, with MnNP-treated infected-plants exhibiting minimal symptoms and reduced invasive fungal biomass in within watermelon tissues. Transcriptomic analysis revealed that MnNPs downregulated genes in the fusaric acid biosynthesis pathway, a key determinant of *Fon* virulence, disrupting its ability to infect host plants. Additionally, MnNPs modulated rhizosphere metabolites, enriching defense-related compounds, including phenolics, flavonoids, and organic acids. These findings establish MnNPs as a robust and impactful strategy for managing Fusarium wilt. By integrating nanotechnology and plant-rhizopshere interactions, this study provides a novel approach to mitigating soilborne diseases, emphasizing the potential of nano-enabled disease management approaches to enhance crop protection and sustainability in agriculture.

*Correspondence:
Yanli Wang
ylwang88@aliyun.com
Jiaoyu Wang
wangjiaoyu78@sina.com; wangjy@zaas.ac.cn

Full list of author information is available at the end of the article

Keywords Fusaric acid, Fusarium wilt, Manganese nanoparticles, Rhizosphere metabolome, Watermelon

Introduction

Nanotechnology offers innovative tools for addressing agricultural challenges, including the management of plant diseases [1, 2, 3]. Although a robust literature is available on the disease-controlling potential of chemically-synthesized nanoparticles (NPs) in various crops such as tomato (*Solanum lycopersicum*), wheat (*Triticum aestivum*), and rice (*Oryza sativa*) [4, 5, 6, 7]; however, earlier studies often reported biocompatibility and environmental safety concerns of conventional chemical-based nano-agrochemicals. For example, chemically-synthesized copper NPs (450 mg/L) reduced root elongation up to 28% through increasing cell wall rigidity in lettuce (*Lactuca sativa* L.) compared with untreated controls [8]. Similarly, chemically-synthesized silver NPs (20 ppm) inihibited the root weight (34%), stem length (43%), and seedling height (40%) in cucumber plants (*Cucumis sativus* L.) than untreated control plants [9]. Recently, biologically-synthesized NPs have garnered significant attention for their eco-friendly and sustainable applications [10, 11]. Biological synthesis methods, especially using bacteria, offer greater functional benefits and biocompatibility to NPs, thus replacing their chemically-synthesized counterparts [12, 13, 14]. Biogenic maganese (Mn) NPs, synthesized through microbial processes, stand out for their remarkable antimicrobial properties and minimal environmental impact. These NPs exhibit potent activity against a range of phytopathogens, including *Fusarium oxysporum* f. sp. *niveum* (*Fon*), watermelon (*Citrullus lanatus* L.) Fusarium wilt pathogen [12, 15]. Their antifungal efficacy is attributed to mechanisms such as disruption of pathogen cell membranes, inhibition of cellular processes, and modulation of oxidative stress [16]. For example, biogenic MnNPs inhibited the growth of bacterial leaf blight pathogen, *Xanthomonas oryzae* pv. *oryzae*, by inducing oxidative damage and deforming cell wall [15]. Unlike conventional fungicides, Mn-based nanoagrochemicals not only mitigate pathogen growth but also augment plant nutrient supply and physiology, improving its growth and development [17]. For example, MnNPs (1 mg/plant) improved the chlorophyll content (~20%) and photosynthesis rate (12%), ehancing the biomass of cucumber plants by ~21% [18]. Given facts suggest biogenic MnNPs as a promising tool for sustainable disease management in agriculture, offering an innovative solution to combat one of the most devastating diseases in watermelon cultivation.

Fon is a significant pathogen of watermelon, causing Fusarium wilt, which results in severe yield losses in this crop globally (up to 100%) [19]. The pathogenicity of this strain is strongly correlated to the production of secondary metabolites, including mycotoxins (such as fusaric acid), effector proteins (such as secreted in xylem), and enzymes (such as cellulases, xylanases, and pectinases) that aid in host tissue colonization and disease progression [20, 21, 22, 23]. These metabolites play essential roles in the physiological processes and virulence of *Fon* by facilitating the breakdown of plant cell walls and enhancing its survival in hostile environments [24, 25]. As watermelon cultivars with inherent resistance to *Fon* are limited, soil treatment with chemical fungicides remain the primary method for managing Fusarium wilt. However, overreliance on these chemical treatments has raised serious environement safety concerns due their off-target effects and excessive buildup in soil, which compromises their repeated application in agriculture fields and exacerbates the problem of mycotoxin accumulation in infected plants [12, 26, 27]. Recent studies suggest that alternative control methods, including the use of multifarious engineered NPs, may provide promising solutions [28, 29, 30]. For example, cerium oxide NPs (250 mg/L) significantly suppressed Fusarium wilt upto 53% by augmenting antioxidative defense machinery (catalase and polyphenol oxidase) in *F. oxysporum* f. sp. *lycopersici*-infected tomato plants [31]. Similarly, 100 µg/mL biogenic magnesium NPs inhibited *Fon* hyphal growth (~40%) by directly disrupting pathogen cell envelope, conidiation, and conidial germination [30]. However, the mechanisms by which they influence secondary metabolite production and fungal virulence remain poorly understood. Given these facts, furture studies should investigate the safety and efficacy of nanomaterials for disease management and to understand their impacts on fungal biology.

Among secondary metabolites, fusaric acid is pivotal for regulating pathogenicity and biology of phytopathogenic fungi [21]. This phytotoxic compound has been shown to contribute to the virulence of *Fon* by impairing biochemical activities in plants such as respiration and nutrient acquisition, thus facilitating fungal infection [32]. Notably, fusaric acid has been implicated in the inhibition of plant immune responses, allowing the fungus to establish and maintain infection within the host [33]. Previous studies have revealed that fusaric acid production is critical for fungal growth and sporulation, and its presence in infected tissues correlates with disease severity. Importantly, fusaric acid has been shown to enhance the ability of *Fusarium* species to colonize plant vascular systems, contributing to the development of wilt diseases [34, 35]. To date, a cluster of 12 fusaric acid biosynthetic (*FUB*) genes has been identified and reported to regulate various physiological and biochemical processes in

phytopathogenic fungi [36]. Studies have indicated that deletion of *FcFUB1* in *Fusarium circinatum* reduced fusaric acid production and pathogenicity on *Pinus patula* [35]. Similarly, in *F. oxysporum* f. sp. *cubense*, disruption of *FocFub4* induced defects in virulence on banana (*Musa* spp.) plants [33]. These findings underscore the pivotal role of fusaric acid in pathogenicity of fungal phytopathogens and highlight its potential as a target for disease control strategies.

During infection, pathogens alter the composition and abundance of rhizosphere metabolites to favor the disease progression [37]. On the other hand, plants release a variety of antimicrobial metabolites, including organic acids, phenolics, and phytohormones, to antagonize pathogen growth or to enhance disease resistance mechanisms. These metabolites, including phenolic compounds, organic acids, and volatile organic compounds, have been shown to either suppress or enhance pathogen growth [38, 39, 40]. Understanding the intricate networks between rhizosphere metabolites and NP-plant-*Fon* triad is vital for developing sustainable crop protection strategies. Although antagonistic potential of metallic NPs against *Fon* has been previously described, the specific molecular mechanisms driving these effects remain largely unexplored. In this study, we biosynthesized MnNPs using cell-free filtrate of a locally-isolated bacterial strain *Lysinibacillus sphaericus* NOTE11, showing higher resistance to Mn-containing precursor salt than other bacterial isolates. Specifically, our study investigated the molecular inhibition mechanism of MnNPs on *Fon*, focusing on their impact on fungal growth and virulence. Transcriptomic and metabolomic studies revealed that MnNPs significantly reduced hyphal growth, conidiation, and conidial germination by dysregulating key *FUB* genes, as well as suppressed *Fon* pathogenicity on watermelon plants by precisely regulating disease-suppressive rhizosphere metabolites. Moreover, we identified that MnNPs induced cellular damage, disrupted cell wall integrity, and inhibited key molecular pathways involved in fungal stress responses. Taken together, our study elucidates the antifungal potential of MnNPs and provides new insights into their molecular mechanisms of action against *Fon*, suggesting a better and sustainable alternative for watermelon Fusarium wilt management.

Materials and methods

Isolation and molecular identification of Mn-resistant bacteria

Bacterial strains resistant to Mn were isolated from the rhizosphere of watermelon plants using the serial dilution method. Briefly, rhizosphere soil samples were serially diluted in sterile saline solution (0.85% w/v) [41]. Aliquots (100 µL) from two different dilutions (i.e., 10^{-3} and 10^{-6}) were plated onto manganese chloride ($MnCl_2.4H_2O$, 99% purity)-supplemented nutrient agar and incubated at 28 ± 2 °C for 72 h. Following incubation, grown bacterial colonies were purified and tested for their resistance to Mn using the minimum inhibitory concentration (MIC) method [42]. To characterize the strains molecularly, *16 S rRNA*, commonly used for bacterial phylogeny, and the RNA polymerase beta subunit (*rpoB*), which provides more specific resolution at the species level, were apmilfied from the extracted DNA with fD1/rD1 and rpoB-F/rpoB-R primer pairs, respectively (Table S1) [43, 44]. The resulting sequences were analyzed using NCBI BLASTn to identify evolutionarily-linked bacterial species. Phylogenetic relationships were then inferred using the maximum likelihood method with bootstrap algorithm (1000 replicates), and evolutionary trees were constructed using MEGA7 software to align the sequences with homologous counterparts.

MnNPs biosynthesis and characterization

MnNPs were extracellularly biosynthesized using the cell-free filtrate of the Mn-resistant strain, as described previously [12]. Briefly, the 2-d old broth culture of Mn-resistant strain was centrifuged (5000×*g*) to obtain the extracellular metabolite-rich supernatant for MnNP synthesis. Following centrifugation, the cell-free filtrate and an equal volume of a Mn precursor solution (0.01 M $MnCl_2.4H_2O$) was co-incubated at 28 ± 2 °C for an additional 72 h, resulting in the formation of MnNPs. The purified MnNPs were freeze-dried, homogenized, and stored in a sealed container for further analysis.

The biosynthesized MnNPs were characterized for their physicochemical properties using a range of analytical techniques, as described previously [45]. Fourier-transform infrared (FTIR) spectroscopy (Thermo Scientific NICOLET iS50FT-IR) was utilized to detect functional groups responsible for stabilizing the MnNPs and their interactions with biomolecules from the culture supernatant, within the 4000–500 cm – 1 spectral range. For analyzing crystallinity and purity of the MnNPs, X-ray diffraction (XRD) analysis was performed using an XPertPro diffractometer (Almelo, the Netherlands). To determine shape, size range, and elemental composition of the MnNPs, energy-dispersive X-ray spectroscopy (EDS; Oxford Instruments, High Wycombe, UK)-coupled scanning electron microscopy (SEM; TM1000, Hitachi, Tokyo, Japan) was employed. For further analyzing ultrastructure and morphology at higher resultion, transmission electron microscopy (TEM; 1230 JEOL, Akishima, Japan) was performed.

In vitro antifungal activity and morphological observations

The antagonistic potential of MnNPs against *Fon* were assessed on solid potato dextrose agar (PDA) media (200 g potato extract, 20 g glucose and 15 g agar per liter

of ddH_2O), with varying concentrations of bio-MnNPs (0, 25, 50, 100 µg/mL) as described previously [12]. The antifungal activity was evaluated by calculating the percentage of growth inhibition based on radial growth diameter on PDA at 9 d post-inoculation (dpi). SEM (TM1000, Hitacchi, Tokyo, Japan) and TEM (1230 JEOL, Akishema, Japan) were used to examine changes in *Fon* morphology after treatment with bio-MnNPs. For microscopic observations, fungal hyphae grown on PDA with or without MnNPs were collected, washed, and processed as described previously [30]. Samples from six individual repeats per treatment were analyzed using TEM/SEM, with at least five fields examined per sample. The effects of bio-MnNPs on *Fon* conidiation, conidial length, conidial morphology, septal number, and germination were also assessed, with control experiments using untreated and bulk Mn-treated *Fon* as described previously [30].

In planta disease and fungal biomass assays

Watermelon plants of a susceptible cultivar (Zaojia) were used for disease assays, as described previously [12]. Briefly, watermelon plants (3-week-old) were root inoculated with the *Fon* inoculum (5×10^5 spores/mL) [46, 47]. The inoculated seedlings were then replanted in fresh potting mix, followed by treatment with 50 mL of MnNPs or bulk Mn (99.8% purity, particle size 60–300 µm) suspensions (100 µg/mL), as described previously [12, 26]. To maintain conditions conducive to disease development, the plants were covered with cling film. Untreated mock-inoculated and *Fon*-inoculated plants served as controls, and disease severity was evaluated at 21 dpi using a previously reported 4-point scale [47].

In planta fungal biomass was assessed following an established protocol [48]. Briefly, watermelon seedlings (3-week-old) treated with or without MnNPs and bulk Mn were exposed to *Fon* inoculum (5×10^5 spores/mL) and maintained at 26 °C under shaking conditions (95 rpm). Plant tissues (roots and stems) were periodically collected (3, 6, and 9 dpi), and relative invasive fungal growth was estimated by quantifying the genomic DNA levels of the *FonOpm12* (*Fon*)/*ClRps10* (watermelon) using qPCR with gene-specific primers (Table S1).

Transcriptomic analysis

The *Fon* cultures were grown in PD broth media with three replicates at 26 ℃ and 250 rpm. At 36 h post-incubation, *Fon* cultures were supplied with MnNPs (100 µg/mL) and incubated for another 12 h. After incubation, untreated and MnNP-treated *Fon* cultures were harvested, frozen in liquid nitrogen, and stored at -80 ℃ for subsequent transcriptome analysis. Solexa sequencing (Illumina) and data analysis were performed by Novogene (Beijing, China). Clean reads without low quality and duplicate sequences were then mapped to the reference genome (PRJNA18813) using TopHat2 software (v2.0.12) [49]. The FPKM (Fragments per Kilobase per Million mapped reads) values indicating gene expression levels were determined using RSEM program [50]. Differentially expressed genes (DEGs), with a fold change ≥ or ≤ 2 and a p-value ≤ 0.05, were determined using the DESeq R package [51]. Kyoto Encyclopedia of Genes and Genomes (KEGG) and Gene Ontology (GO) enrichment analyses of the DEGs were conducted using the KEGG database (http://www.genome.jp/kegg/) and GOseq R package, respectively [52].

Generation of targeted deletion mutants and comparative growth assays

Gene replacement fragments for *FonFUB5*, *FonFUB8*, *FonFUB11*, and *FonFUB12* were constructed by amplifying their 5′ and 3′ flanking regions using specific primers (Table S1) and fusing them with a hygromycin-resistant cassette (*HPH*) through overlap polymerase chain reaction (PCR) as described previously [53]. The purified constructs were introduced into wild-type (WT) protoplasts following previously established protocols. Positive transformants were selected on PDA plates containing hygromycin B (100 µg/mL) and verified through PCR using primers listed in Table S1.

For comparative growth assays, WT and deletion mutants were grown on PDA plates supplied with MnNPs, bulk Mn, or sterile ddH_2O (controls) and alterations in growth rates were measured at 9 dpi.

Metabolomic profiling of rhizosphere soil

Non-targeted metabolomic analysis of healthy and *Fon*-infected rhizosphere soil samples supplied with or without MnNPs was conducted by Central Laboratory of Zhejiang Academy of Agricultural Sciences, State Key Laboratory for Managing Biotic and Chemical Threats to the Quality and Safety of Agro-products (Hangzhou, China) using gas chromatography-mass spectrometry (GC–MS) as described previously [54]. To ensure accuracy, quality control (QC) samples were included every 10 samples, prepared by pooling equal amounts of extract from each sample. The analysis was performed on a 7890B-5977 A GC/MS instrument (Agilent Technologies Inc., Santa Clara, CA, USA). Raw data were converted to mzXML format using Proteo Wizard software (version 3.0.8789), and batch effects were minimized by normalization with QC samples. Metabolites with a relative standard deviation exceeding 30% in the QC samples were excluded from further analysis.

Data profiling was performed by Central Laboratory of Zhejiang Academy of Agricultural Sciences (Hangzhou, China). Molecular weights were determined using mass-to-charge ratios (m/z) of parent ions, with molecular

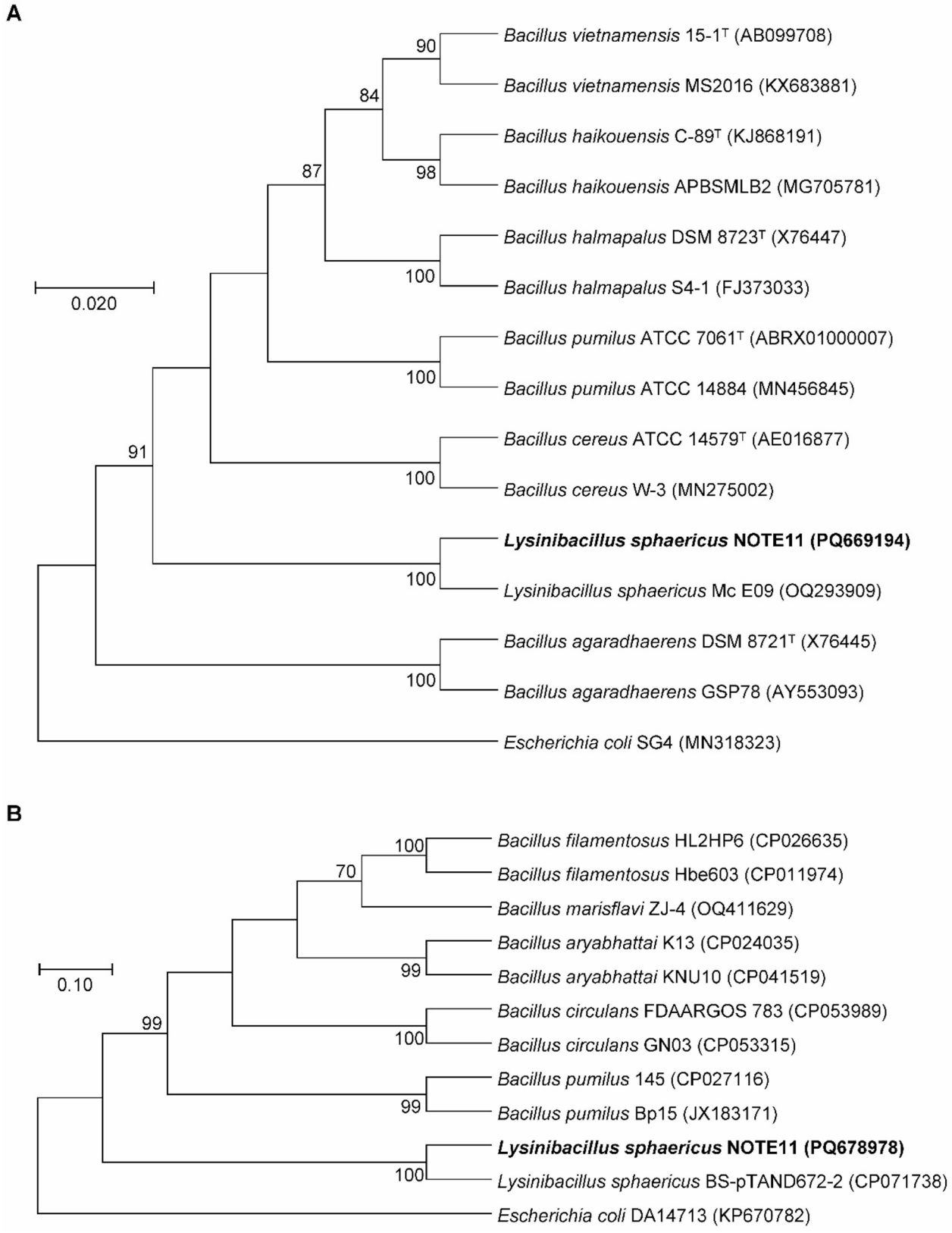

Fig. 1 (See legend on next page.)

(See figure on previous page.)

Fig. 1 Phylogenetic classification of bacterial strains based on *16S rRNA* and *rpoB* gene sequences. (**A**) Phylogenetic tree constructed using the *16S rRNA* gene sequences, showing the evolutionary relationship of the bacterial isolate with closely related strains from the genus *Bacillus* and *Lysinibacillus*. The tree was constructed using the maximum likelihood (ML) method with bootstrap values (> 50) indicated at branch nodes (percentage of 1,000 replicates). The scale bar represents the number of nucleotide substitutions per site. (**B**) Phylogenetic tree constructed based on the *rpoB* gene sequences. showing the evolutionary relationship of the bacterial isolate with closely related strains from the genus *Bacillus* and *Lysinibacillus*. The tree was constructed using the ML method with bootstrap values (> 50) indicated at branch nodes (percentage of 1,000 replicates). The scale bar represents the number of nucleotide substitutions per site. *Escherichia coli* served as an outgroup in both trees

formulas predicted based on parts per million (ppm) and adduct ions. These were compared against database entries for identification through MS analysis. Fragment ion matching from MS/MS data provided further confirmation. Differentially abundant metabolites (DAMs) were analyzed using Metabo Analyst, and metabolic pathways were visualized using the KEGG Mapper tool, referencing the National Institute of Standards and Technology (NIST) standard spectrum.

RNA extraction and expression analysis

RNA extraction was carried out using TRIzol reagent (Vazyme Biotech, Nanjing, China), and complementary DNA (cDNA) was synthesized with the HiScript II QRT SuperMix kit (Vazyme Biotech, Nanjing, China). Quantitative PCR (qPCR) reactions were prepared using AceQ qPCR SYBR Green Master Mix (Vazyme Biotech, Nanjing, China) and performed on a 7500 Fast Real-Time System (Applied Biosystems, Foster City, CA, USA). Gene expression levels were normalized against *FonActin* using the $2^{-\Delta\Delta CT}$ method to calculate the relative expression of target genes [55]. The primers used for this analysis are listed in Table S1.

Statistical analysis

Data were using one-way analysis of variance (ANOVA) with Data Processing System (DPS) package. Statistical significance was evaluated at a p-value threshold of ≤ 0.05 using the Least Significant Difference (LSD) test [56]. Results are presented as the mean ± standard deviation (SD) derived from three independent replicates.

Results

Mn-resistant strain isolation and molecular characterization

Here, a highly Mn-resistant bacterial strain, designated NOTE11, was identified, exhibiting a high MIC of 12 mM against $MnCl_2.4H_2O$ (Table S2). The sequences of *16S rRNA* (Accession no. PQ669194) and *rpoB* (Accession no. PQ678978) taxonomically classified strain NOTE11 as *Lysinibacillus sphaericus*. Sequence analysis revealed 99.80% similarity in the *16S rRNA* gene with *L. sphaericus* Mc E09 (OQ293909) and 100% similarity in the *rpoB* gene with *L. sphaericus* BS-pTAND672-2 (CP071738). Phylogenetic analysis of both taxonomic marker genes (*16 S rRNA* and *rpoB*) indicated a evolutionary correlation among strain NOTE11 and other *L. sphaericus* and *Bacillus* spp. (Fig. 1A, B). These findings establish the taxonomic identity of strain NOTE11 as *L. sphaericus*.

Morpho-physicochemical properties of MnNPs

Here, cell-free filtrate from *L. sphaericus* NOTE11 successfully biosynthesized MnNPs. The MnNPs synthesis was visually confirmed by a distinct color change in the reaction mixture from pale yellow to dark brown, indicating the reduction of Mn ions and the subsequent formation of MnNPs. FTIR analysis identified characteristic absorption bands at 789, 1143, 1624, 2351, 3423, and 3645 cm^{-1}, indicating the presence of diverse functional groups over the MnNP surface, such as C-H bending, C-N stretching, C = C stretching, O = C = O stretching, O-H stretching (alcohol), and O-H stretching (water) (Fig. 2A). These findings suggest that biomolecules in the bacterial culture supernatant play a crucial role in the biosynthesis and stabilization of MnNPs. The crystalline strucutre of biosynthesized MnNPs was confirmed by XRD analysis, showing specific diffraction peaks at 2θ, including 24.16°, 31.36°, 37.29°, 41.49°, and 56.17°, corresponding to the (101), (201), (210), (211), and (212) planes of crystalline Mn, respectively (Fig. 2B). SEM imaging revealed predominantly spherical MnNPs with an irregular morphology and an average particle size of approximately 32.28 nm (Fig. 2C). TEM further verified the spherical shape and uniform dispersion of MnNPs, exhibiting a narrow size range (Fig. 2D). EDS analysis depicted chemical constituents of the MnNPs, showing distinct peaks for Mn (30.26%) and O (oxygen; 63.78%) (Fig. 2E), indicating that the MnNPs consist primarily of Mn and O. These comprehensive characterizations provide a detailed understanding of the physicochemical properties and structural features of MnNPs, which were biosynthesized using the cell-free filtrate of *L. sphaericus* NOTE11.

MnNPs disrupt *Fon* fundamental biological functions

In vitro antifungal assays demonstrated that varying levels of MnNPs (except 25 µg/mL) significantly disrupted hyphal growth than bulk Mn-treated and untreated *Fon*. Biogenic MnNPs (100 µg/mL) highly reduced *Fon* hyphal growth by 21.97% on PDA, in contrast to untreated controls (Fig. 3A-C). Morphological observations of *Fon* treated with MnNP (100 µg/mL) revealed noticeable alterations in hyphal structure and morphology, including abnormal branching, distorted surfaces, and

compromised cellular structure, indicative of cellular damage and cytoplasmic leakage. In contrast, 100 µg/mL bulk Mn-treated and untreated *Fon* samples exhibited intact hyphal and cellular structures (Fig. 3D).

Moreover, MnNP treatments at different concentrations (25, 50, and 100 µg/mL) significantly reduced conidial morphogenesis, germination rate, and septation than bulk Mn-treated and untreated *Fon*. Specifically, 100 µg/mL MnNP-treated *Fon* produced significantly less conidia (63.20%) at 24 h post-treatment compared to untreated *Fon* (Fig. 4A). The conidial germination rate was also notably decreased (10%) in *Fon* condial suspesion supplied with 100 µg/mL MnNP, whereby 100 µg/mL bulk Mn-treated and untreated controls showing a germination rate of around 65% and 90%, respectively (Fig. 4B, C). Calcofluor white staining and microscopic observation revealed that *Fon* cultures treated with varying MnNPs concentrations (50 and 100 µg/mL) produced macroconidia with no or 1 septum, whereas bulk Mn-treated and untreated *Fon* produced macroconidia with 1 to 3 septa (Fig. 4D, E). Additionally, majority of the macroconidia from 100 µg/mL MnNP-treated *Fon* were significantly shorter than untreated controls (Fig. 4F). These results underscore the promissing *Fon*-suppressing potential of biogenic MnNPs, deciphering their significant impact on key pathogen biological processes such as conidiation, spore germination, and conidial morphology.

MnNPs suppressed Fusarium wilt and invasive fungal growth

In this study, we assessed the effectiveness of biogenic MnNPs (100 µg/mL) and bulk Mn (100 µg/mL) in controlling watermelon Fusarium wilt. Disease assays demonstrated significantly reduced disease severity in MnNP-treated plants than bulk Mn-treated and untreated *Fon*-infected controls (Fig. 5A–C). Notably, the proportion of healthy plants with no or minor chlorosis symptoms was notably higher in the MnNP-treated group (~ 88.89%) than bulk Mn-treated (22.22%) and untreated *Fon*-infected controls (11.11%) (Fig. 5B). Specifically, MnNP-treated plants exhibited a significantly lower disease severity index (DSI = 14.36) with minimal or no disease appearance than bulk Mn-treated (DSI = 85.01) and untreated *Fon*-infected plants (DSI = 88.38) (Fig. 5C). These results demonstrate the promissing disease-suppressive potential of biogenic MnNPs, especially for watermelon Fusarium wilt management.

We also examined the impact of MnNPs and bulk Mn at 100 µg/mL concentration on invasive pathogen growth within watermelon tissues. The results showed that MnNP treatment resulted in the most significant reduction in fungal biomass in both root and stem tissues, compared to bulk Mn treatment and untreated *Fon*-infected controls. Specifically, at 6 dpi, MnNP-treated plants showed significantly reduced fungal biomass in roots and stems (41.57% and 68.89%, respectively), than untreated *Fon*-infected controls (Fig. 5D, E). In contrast to bulk Mn, MnNP treatment showed the highest reduction in fungal biomass at 9 dpi, with a 51.70% reduction in roots and 67.62% in stems (Fig. 5D, E). These data clealry depict the superior efficacy of MnNPs in controlling watermelon Fusarium wilt, precisely by inhibiting the accumulation of fungal biomass in plant tissues.

MnNPs induced transcriptomic alterations in *Fon*

To investigate the potential inhibitory molecular mechanisms of MnNPs against *Fon*, transcriptomic changes in the MnNP-treated and untreated *Fon* were compared using the RNA-seq technique. A total of 649 DEGs, comprising 137 upregulated and 512 downregulated genes (with a fold change ≥ or ≤ 2 and a p-value ≤ 0.05), were identified in MnNP-treated *Fon* (Table S3 and Table S4; Fig. S1).

A total of 76 KEGG pathways (17 upregulated and 59 downregulated) were identified in the MnNP-treated *Fon* (Fig. 6A, B). Notably, the largest group of pathways included Starch and sucrose metabolism (3/3 upregulated/downregulated DEGs), followed by Nitrogen metabolism (2/2 upregulated/downregulated DEGs), ABC transporters (2/2 upregulated/downregulated DEGs), Nucleocytoplasmic transport (2/2 upregulated/downregulated DEGs), Meiosis-yeast (2/2 upregulated/downregulated DEGs), and Biosynthesis of amino acids (2/2 upregulated/downregulated DEGs) (Fig. 6A, B). In addition, GO analysis categorized the upregulated and downregulated DEGs into three main functional groups: molecular function, cellular component, and biological process (Fig. 6C, D). Both upregulated and downregulated DEGs were significantly enriched in regulation of binding of carbohydrate, cofactor and coenzyme, formation of intracellular organelles, and regulation of gene expression or stress responses at the molecular, cellular, and biological levels, respectively, compared to the untreated controls (Fig. 6C, D). Overall, the findings suggest that MnNPs induce significant transcriptomic changes in *Fon*, particularly in pathways related to growth, cell division, and virulence.

MnNPs dysregulated fusaric acid biosynthetic pathway to inhibit *Fon* growth and pathogenicity

Further analysis of the RNA-seq data from MnNP-treated *Fon* revealed numerous mycotoxin production-related DEGs involved in the fusaric acid biosynthesis pathway, such as *FonFUB5* (FOXG_15243; downregulated), *FonFUB8* (FOXG_17660; downregulated), *FonFUB11* (FOXG_17181; downregulated) (Table S4), and *FonFUB12* (FOXG_15235; upregulated) (Table S3), which

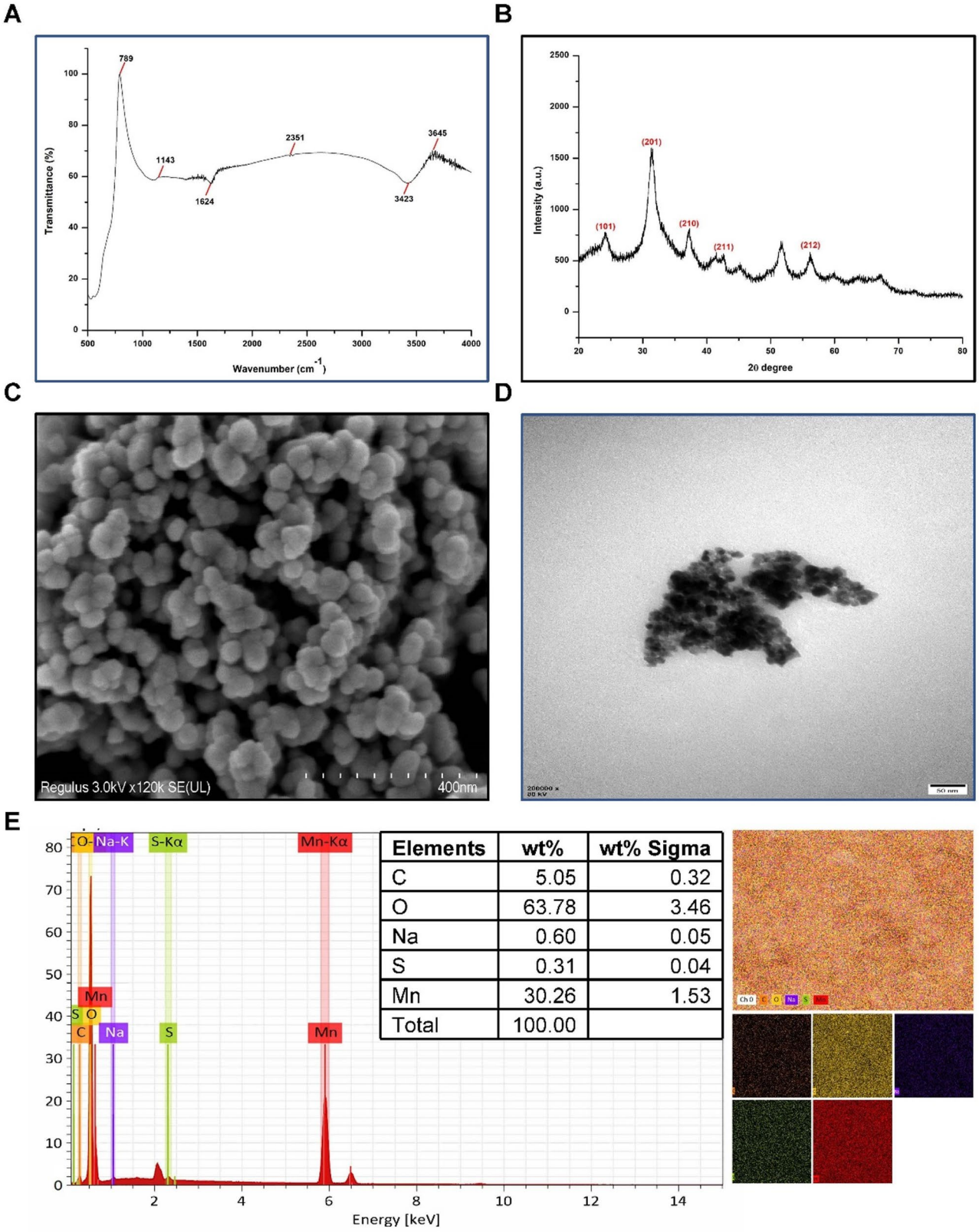

Fig. 2 Characterization of biosynthesized MnNPs. (**A**) FTIR spectrum showing the functional groups involved in MnNP synthesis. (**B**) XRD pattern confirming the crystalline structure of MnNPs. Prominent diffraction peaks validate the formation of MnNPs crystals. (**C**) SEM image revealing the spherical morphology of MnNPs with uniform size distribution at the nanoscale. (**D**) TEM image showing well-dispersed MnNPs with aggregated clusters, further confirming nanoscale size. (**E**) EDS analysis (*left*) and elemental mapping (*right*) highlighting the elemental composition of MnNPs

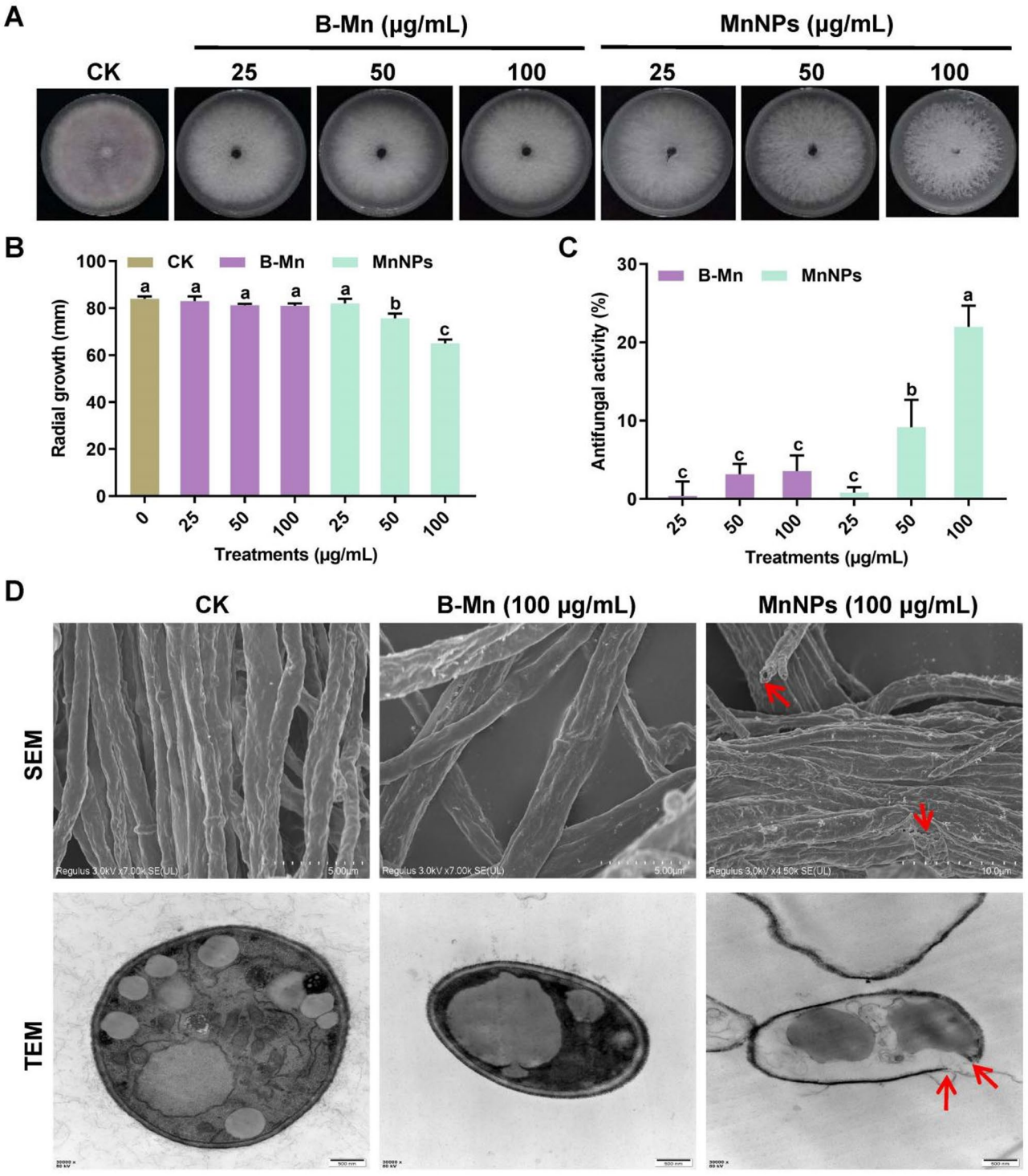

Fig. 3 Antifungal potential of MnNPs against *Fon*. (**A**) Radial growth of *Fon* on PDA plates supplemented with different concentrations (25, 50, and 100 µg/mL) of bulk Mn (B-Mn) and MnNPs. Control (CK) plates show normal fungal growth without any treatment. (**B**) Quantitative measurement of radial growth (mm) at varying concentrations of B-Mn and MnNPs. Different letters above bars represent significant differences (p-value ≤ 0.05). (**C**) Antifungal activity (%) of B-Mn and MnNPs. (**D**) Microscopic analysis of fungal structures treated with MnNPs (100 µg/mL). SEM images (*upper panel*) reveal damage to fungal hyphae, including irregular morphology and structural disruption (*red arrows*), compared to intact hyphae in CK and B-Mn-treated samples. TEM images (*lower panel*) highlight intracellular damage in MnNP-treated fungal cells, including vacuolization, disrupted cell membranes (*red arrows*), while CK and B-Mn treatments show intact cellular ultrastructure

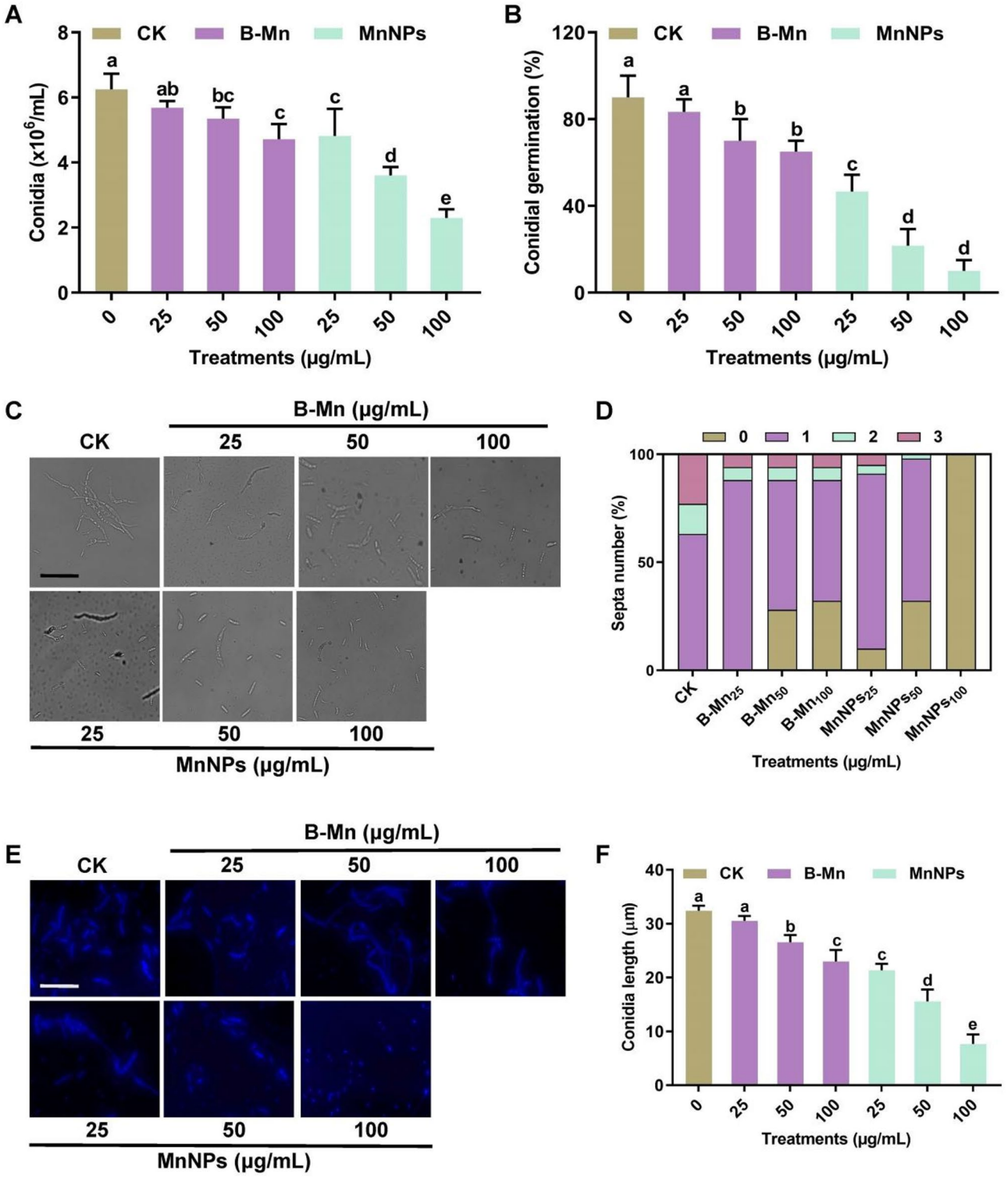

Fig. 4 Effect of MnNPs on fundamental biological processes in *Fon*. (**A**) Macroconidia production by *Fon* in MBL medium supplemented with or without MnNPs and bulk Mn (B-Mn). (**B**) Conidial germination rate and (**C**) germinated conidia micrograph [scale bar = 20 µm] of *Fon* in YEPD medium supplemented with or without MnNPs and B-Mn. Atleast 100 spores per field were observed for estimating conidial germination rates. (**D**) Septa number, (**E**) macroconidial morphology [scale bar = 20 µm], and (**F**) conidia length with or without MnNPs and B-Mn. Different letters above bars represent significant differences (p-value ≤ 0.05)

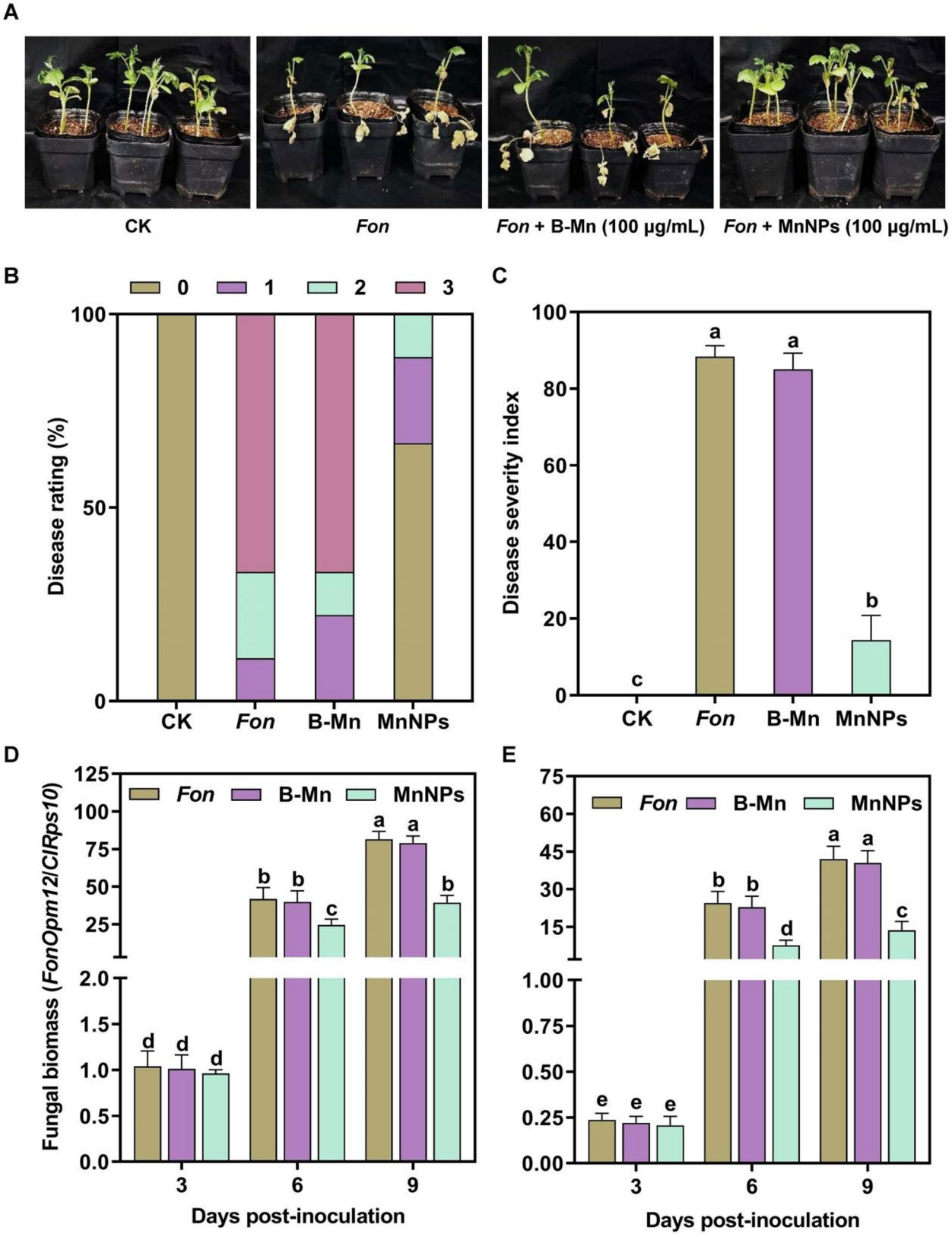

Fig. 5 MnNPs-induced suppression of fungal biomass reduce *Fon* pathogenicity on watermelon. (**A**) Disease phenotype of plants supplied with or without MnNPs at 21 dpi. (**B**) Disease scores and (**C**) disease severity indexes of *Fon*-infected plants supplied with or without MnNPs at 21 dpi. Invasive fungal growth in (**D**) roots and (**E**) stems of *Fon*-infected plants supplied with or without MnNPs. Different letters above bars represent significant differences (p-value ≤ 0.05)

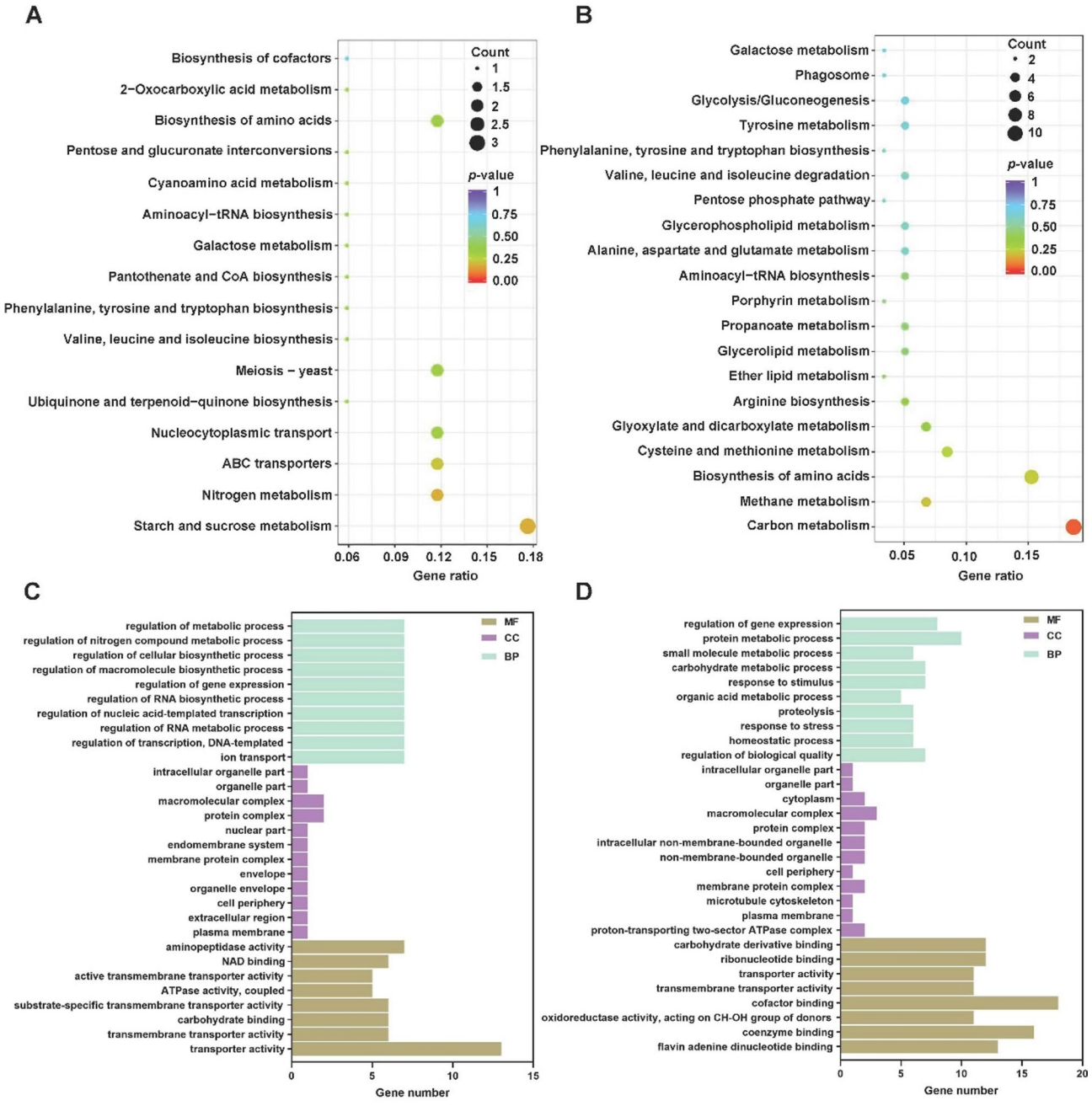

Fig. 6 MnNPs-induced transcriptomic alterations in *Fon* suprress its growth, development, and pathogenicity. Highly enriched (**A**) upregulated and (**B**) downregulated KEGG pathways in MnNPs-treated *Fon*. The size of each circle represents gene number involved in the corresponding pathway. The gene ratio of a pathway was represented as the ratio of the number of DEGs (p-value ≤ 0.05) to the total number of background genes in the corresponding particular pathway. GO annotation for (**C**) upregulated and (**D**) donwregulated DEGs in MnNPs-treated *Fon*. In the plots, y-axis represents roles of the DEGs at different levels of biological activity, while x-axis represents number of genes involved in corresponding function

are known to play key roles in pathogen biology and virulence on host plants.

To investigate the regulatory roles of *FonFUB* genes in *Fon*, we analyzed the expression of *FonFUB5*, *FonFUB8*, *FonFUB11*, and *FonFUB12* across different developmental stages and in infected watermelon roots. The results demonstrated that *FonFUB5*, *FonFUB8*, *FonFUB11*, and *FonFUB12* expression level was significantly higher in germinating conidia than that in mycelia and conidia at 12 h post-inoculation (hpi) (Fig. 7A–D). Additionally, a substantial upregulation of these genes was observed in infected watermelon roots at 3 dpi (Fig. 7A–D), suggesting a critical role of *FonFUB* genes at the early infection development stages, such as root penetration and

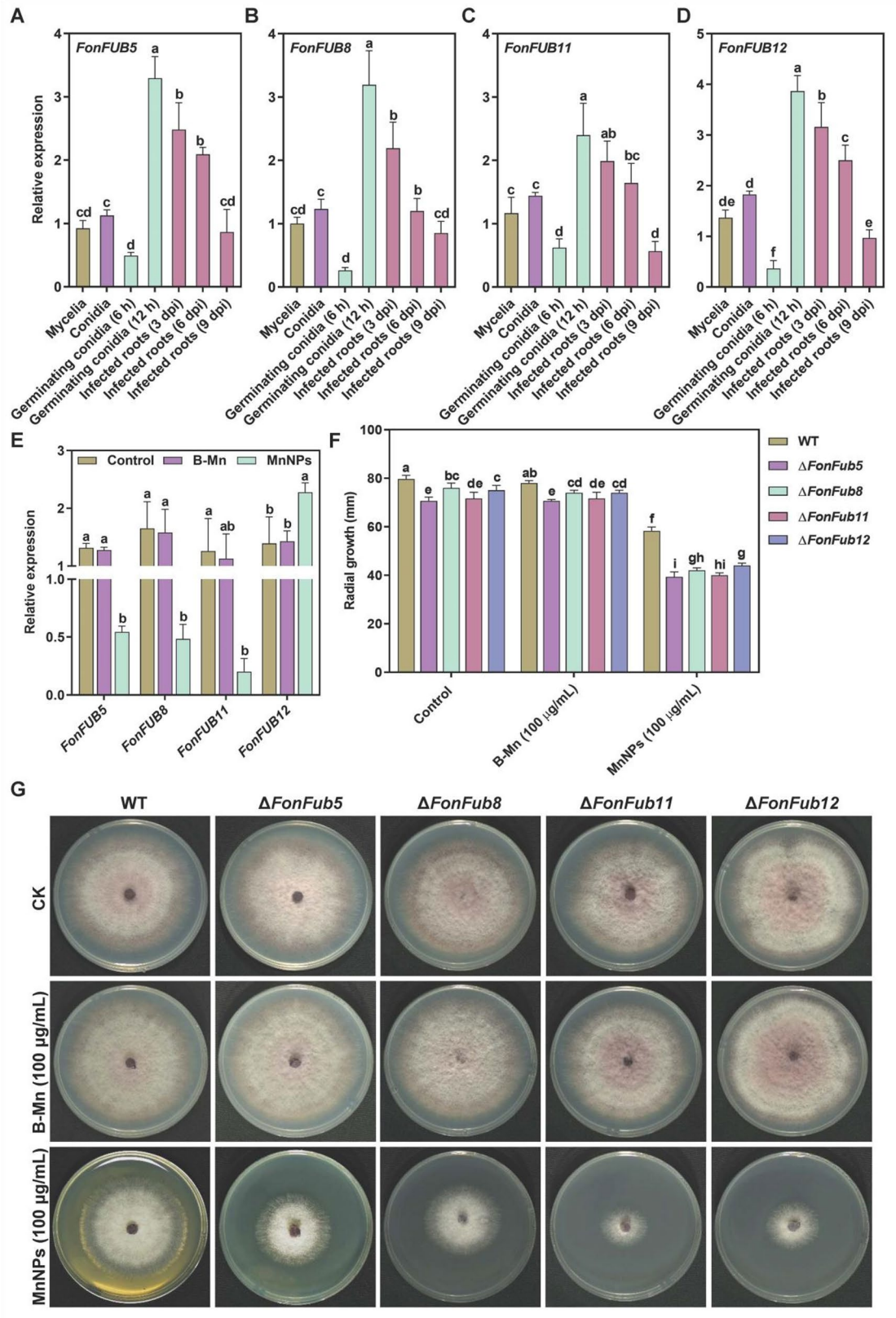

Fig. 7 (See legend on next page.)

(See figure on previous page.)

Fig. 7 MnNPs-mediated dysregulation of fusaric acid biosynthesis genes, *FonFUB5*, *FonFUB8*, *FonFUB11*, and *FonFUB12*, inhibit physiological and pathogenicity-related processes in *Fon*. Expression profiling of (**A**) *FonFUB5*, (**B**) *FonFUB8*, (**C**) *FonFUB11*, and (**D**) *FonFUB12* in mycelia, conidia, germinating conidia, and infected watermelon roots. (**E**) Expression levels of *FonFUB5*, *FonFUB8*, *FonFUB11*, and *FonFUB12* in *Fon* grown with or without MnNPs and bulk Mn (B-Mn). (**F**) Radial growth diameters and (**G**) colony phenotype of *Fon* strains (WT, Δ*FonFub5*, Δ*FonFub8*, Δ*FonFub11*, and Δ*FonFub12*) grown with or without MnNPs and B-Mn. Different letters above bars represent significant differences (p-value ≤ 0.05)

colonization. These data indicate that *FonFUBs* function in regulating the development and pathogenicity of *Fon* in watermelon.

Further, we verify the impact of MnNPs (100 µg/mL) on the expression of *FonFUB5*, *FonFUB8*, *FonFUB11*, and *FonFUB12*. The results showed a significant downregulation of *FonFUB5*, *FonFUB8*, and *FonFUB11* and a notable upregulation of *FonFUB12* following MnNP treatment than bulk Mn-treated and untreated *Fon* (Fig. 7E), which coincide with the RNA-seq data. This suggests that MnNPs may dysregulate these genes involved in fusaric acid biosynthesis, potentially affecting *Fon* pathogenicity.

FonFUB genes regulate MnNPs sensitivity in *Fon*

To investigate the involvement of *FonFUB* genes in regulating the sensitivity response of *Fon* to MnNPs, we assessed the impact of MnNPs (100 µg/mL) on the radial growth of deletion mutants Δ*FonFub5*, Δ*FonFub8*, Δ*FonFub11*, and Δ*FonFub12*, which were confirmed using PCR-based detection (Fig. S2). Notably, in the absence of MnNPs, the deletion mutants showed significantly less hyphal growth compared to the WT, confirming their critical role in *Fon* growth. Intriguingly, the deletion mutants showed greater sensitivity to MnNPs treatment with significantly less hyphal growth than bulk Mn-treated and untreated *Fon* strains (Fig. 7F, G). Specifically, hyphal growth of MnNP-treated Δ*FonFub5*, Δ*FonFub8*, Δ*FonFub11*, and Δ*FonFub12* was significantly reduced by ~44%, ~45%, ~44%, and 41%, respectively, than untreated deletion mutant strains. These findings suggest that fusaric acid biosynthesis genes, including *FonFUB5*, *FonFUB8*, *FonFUB11*, and *FonFUB12*, are likely involved in the stress sensitivity response to MnNPs in *Fon*, indicating their dysregulation is one of the antifungal mechanisms of MnNPs in controlling Fusarium wilt in watermelon.

MnNPs altered rhizosphere metabolites to suppress *Fon* pathogenicity in watermelon

Metabolomic profiling revealed significant shifts in rhizosphere metabolites in response to MnNP treatment in both healthy and *Fon*-inoculated soils. A total of 215 metabolites were identified and categorized into 12 chemical classes, with fatty acyls (19.5%), glycerophospholipids (14.6%), and phenol lipids (14%) being the most prominent groups (Fig. 8A). PCA demonstrated clear clustering of CK, CK + NP, *Fon*, and *Fon* + NP groups along PC1 (45% variance explained), indicating distinct metabolic shifts induced by MnNPs and *Fon* infection. The distinction between *Fon* + NP and *Fon* along PC1 and PC2 suggests that MnNP treatment significantly alters the metabolic landscape in *Fon*-infected soils (Fig. 8B). Notably, MnNP treatment (*Fon* + NP) altered the metabolome of *Fon*-inoculated soils, as evidenced by a unique set of DAMs compared to untreated *Fon* (Fig. 8C, D). Volcano plots highlighted significant enrichment of defense-related metabolites, including spriamycin iii and rubromycin ca1, in MnNP-treated soils (Fig. 8D). Heatmap analysis further corroborated the differential abundance of key metabolites, such as alpha-elaterin 2-d-glucopyranoside acid and hexosylsphingosine, which were elevated in the *Fon* + NP group (Fig. 8E). Pathway enrichment analysis revealed that MnNPs upregulated key metabolic pathways, including glycerophospholipid metabolism, biosynthesis of unsaturated fatty acids, and phenylalanine, tyrosine, and tryptophan biosynthesis, all of which are integral to plant defense and stress signaling (Fig. 8F). Collectively, these findings indicate that MnNPs modulate rhizosphere metabolites to enhance soil health and suppress *Fon* pathogenicity in watermelon.

Discussion

Fusarium wilt fungus, *Fon*, remains one of the most devastating soilborne pathogens affecting watermelon crops worldwide, necessitating innovative and sustainable control strategies. In this study, we explored the potential of MnNPs, derived from *L. sphaericus* NOTE11 culture supernatant (Figs. 1 and 2), as a potent antifungal agent to combat *Fon*, demonstrating their superior efficacy in inhibiting fungal growth, suppressing Fusarium wilt, and modulating rhizosphere metabolites compared to bulk Mn. Previous studies have reported the antifungal activities of various metallic NPs, such as silver and magnesium NPs, against *F. oxysporum* (including *Fon*), largely attributing their effects to oxidative stress induction and disruption of fungal membrane integrity [57, 58]. However, these studies primarily focused on in vitro effects without addressing the potential *in planta* applications or the underlying molecular mechanisms. In contrast, our study not only demonstrated significant inhibitory effects of MnNPs on *Fon* growth and conidiation but also revealed their ability to dysregulate key virulence pathways, including fusaric acid biosynthesis, and suppress fungal biomass accumulation in watermelon plants. Furthermore, the transcriptomic and metabolomic analyses highlighted the multifaceted impact of MnNPs on *Fon*

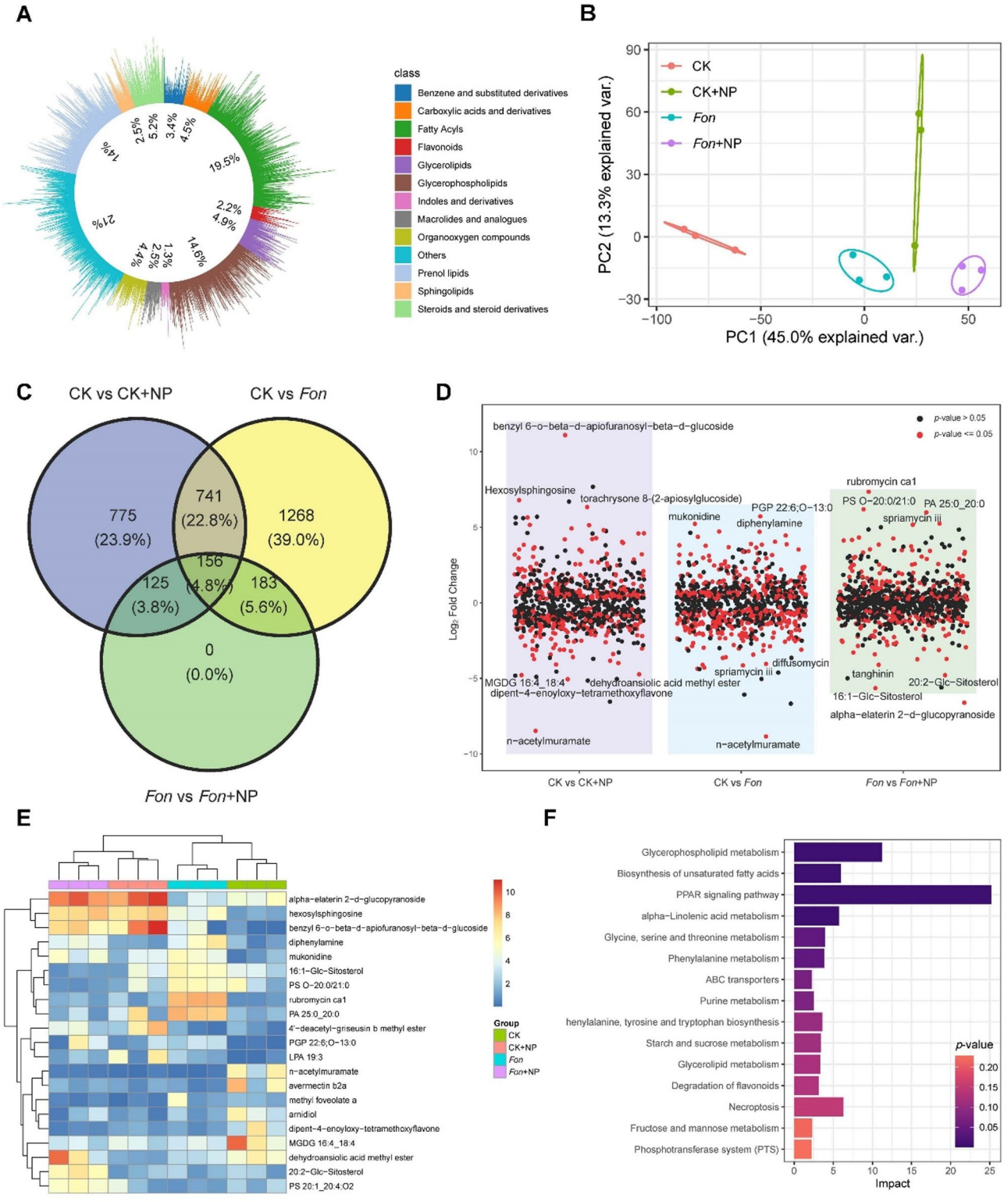

Fig. 8 MnNP-induced shifts in rhizosphere metabolomics suppress *Fon* pathogenicity. (**A**) Classification of identified metabolites into major chemical classes. (**B**) PCA plot depicting distinct metabolic profiles among MnNP-treated or untreated heathy and *Fon*-infected groups. (**C**) Venn diagram showing overlap of DAMs across MnNP-treated or untreated heathy and *Fon*-infected groups. (**D**) Volcano plots of DAMs highlighting significant metabolites in MnNP-treated or untreated heathy and *Fon*-infected groups. (**E**) Heatmap showing the relative abundance of key metabolites across MnNP-treated or untreated heathy and *Fon*-infected groups. (**F**) KEGG pathway analysis indicating enrichment of key metabolic pathways in MnNP-treated or untreated heathy and *Fon*-infected groups

physiology and soil health, underscoring their novelty in modulating host-pathogen interactions and rhizosphere dynamics.

The comprehensive characterization of biosynthesized MnNPs provides valuable insights into their physicochemical and structural attributes, which are crucial for understanding their stability and functionality. The presence of diverse functional groups, as indicated by FTIR analysis, suggests the involvement of biomolecules from *L. sphaericus* NOTE11 in the reduction, capping, and stabilization of MnNPs, contributing to their dispersity and overall functionality [59]. The XRD, microscopic and EDS analyses revealed the crystalline nature of MnNPs, which were predominantly spherical with slight irregularities and showed Mn or O as their active ingredients, consistent with previous reports on biosynthesized metal NPs [12, 45]. These findings collectively establish a strong foundation for understanding the structural and functional properties of MnNPs, supporting their role in plant disease suppression.

The biogenic MnNPs exhibited significant antifungal activity by disrupting fundamental biological processes in *Fon*, including hyphal growth, conidiation, and conidial germination, all of which are critical for fungal development and pathogenicity. Fungal growth, conidiation, spore length, and germination rates were also notably suppressed in MnNP-treated *Fon*, with treated macroconidia exhibiting reduced septation (Figs. 3 and 4), suggesting impaired cellular division and spore viability. These inhibitory effects on basic fungal biological processes can directly be corelated to a weakened ability of *Fon* to establish infection, thereby reducing its pathogenicity in host plants (Fig. 5). Previous studies have highlighted the antifungal properties of metallic NPs, such as zinc-copper oxide NPs (1000 µg/mL) and chitosan-silver NPs (25 mg in 5 mL acetic acid), against phytopathogenic *F. oxysporum* [60, 61]. These NPs primarily exert their effects through mechanisms such as oxidative damage and membrane disruption [62]. However, unlike the non-specific oxidative stress mechanisms reported in these studies, our findings demonstrate that MnNPs not only damage fungal cellular structures but also interfere with key developmental processes like conidiation and septation even at lower concentrations (i.e. 100 µg/mL), as supported by our previous results [12]. Intriguingly, the proficient antifungal activity of MnNPs can be attributed to the biomolecule-assisted synthesis of MnNPs, which could introduce additional functional groups that amplify their antifungal properties [30]. These findings provide deeper insights into the antifungal potential of MnNPs and highlight their primary mechanism of action against *Fon*.

The transcriptomic analysis revealed that MnNPs dysregulated key pathways in *Fon*, particularly those associated with virulence and pathogenicity, such as the fusaric acid biosynthesis pathway (Fig. 6). Several key genes in this pathway, including *FonFUB5*, *FonFUB8*, and *FonFUB11*, were significantly downregulated following MnNP treatment, while *FonFUB12* was upregulated. These genes are critical regulators of fusaric acid production, a mycotoxin known to play a central role in suppressing host defenses and promoting fungal colonization [63, 64]. The observed suppression of *FonFUB* genes in MnNP-treated *Fon* suggests a direct impact on its ability to produce fusaric acid, thereby reducing its pathogenic potential (Fig. 7). Previous studies have established the role of fusaric acid in fungal virulence [33, 34, 65], with research showing that disruption of fusaric acid biosynthesis genes, such as *FUB1*, *FUB2*, *FUB3*, *FUB4*, *FUB5*, and *FUB10*, reduces the aggressiveness of pathogens like *F. oxysporum* f. sp. *cubense TR4* on banana plants [66]. While earlier work has primarily focused on genetic knockouts or chemical inhibitors to suppress fusaric acid production, this study uniquely demonstrates that MnNPs can achieve similar outcomes by directly modulating the expression of fusaric acid biosynthesis genes (Fig. 7). Notably, our results also show that the deletion mutants Δ*FonFub*s exhibited heightened sensitivity to MnNPs (Fig. 7), further highlighting the importance of this pathway in regulating stress response and survival under MnNP treatment in *Fon*. Additionally, our findings extend beyond toxin suppression, as we show that MnNPs also alter the broader transcriptomic landscape of *Fon*, including pathways involved in stress responses, carbohydrate metabolism, and cell division (Fig. 6). Unlike chemical inhibitors that target specific biosynthetic pathways, MnNPs appear to have a more comprehensive impact, simultaneously disrupting multiple facets of fungal metabolism and virulence. This broader mode of action distinguishes MnNPs from traditional antifungal approaches, making them a more robust alternative for managing *Fon* infections.

Previous studies have established that rhizosphere metabolites suppress plant diseases directly by inhibiting the growth or pathogenicity of phytopathogens, including fungi, and indirectly by enhancing plant immunity, thereby maintaining a healthy soil ecosystem for better plant growth and development [40, 67, 68]. Previously, key metabolites involved in defense pathways, including ABC transporters, biosynthesis of antibiotics, and biosynthesis of phenylpropanoids, in tabacco (*Nicotiana tabacum*) against bacterial wilt pathogen, *Ralstonia solanacearum*, were found to be enriched in disease-suppressive rhizospheric soils [69]. In this study, metabolomic analysis revealed that MnNPs significantly altered the metabolic profile of the watermelon rhizosphere, promoting the accumulation of specific secondary metabolites with antifungal properties (Fig. 8). Key metabolites,

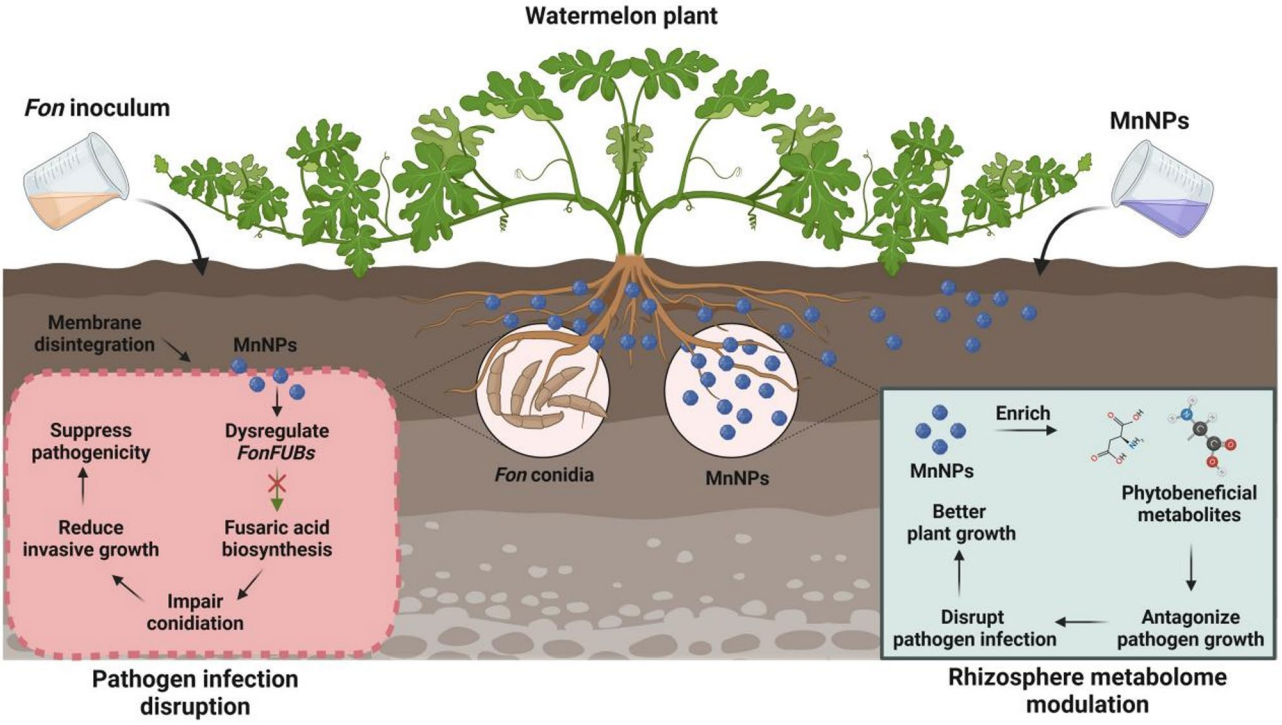

Fig. 9 Proposed model of mechanism of action of MnNPs against *Fon*-induced Fusarium wilt in watermelon. MnNPs enter *Fon* cells by disintegrating membrane, followed by fusaric acid biosynthesis genes (*FonFUB5*, *FonFUB8*, *FonFUB11*, and *FonFUB12*) interruption and conidiation disruption, thereby reducing invasive fungal growth within plant tissues. These events collectively contribute to compromised *Fon* infection and pathogenicity on watermelon plants. Further, MnNPs modulate the rhizosphere metabolome, enriching phytobeneficial metabolites in the root-vicinal area that antagonize pathogen growth and promote plant health. This dual-action mechanism effectively controls *Fon* infection and enhances watermelon resistance to Fusarium wilt

including phenolic compounds, flavonoids, and organic acids, were enriched in MnNP-treated rhizosphere samples (Fig. 8). These metabolites are known to strengthen plant defense mechanisms by directly inhibiting fungal growth or modulating plant-pathogen interactions [70, 71, 72]. For instance, phenolics and flavonoids, which were elevated in the MnNP-treated rhizosphere, have been reported to inhibit the growth and the biosynthesis of the phytotoxins beauvericin and fusaric acid in banana wilt fungus *F. oxysporum* f. sp. *cubense* TR4 [70]. The increased abundance of these metabolites likely contributed to the reduced pathogenicity of *Fon* observed in MnNP-treated plants. Moreover, the presence of these antifungal metabolites may create an unfavorable environment for fungal colonization, thereby indirectly supporting plant health. For example, biogenic selenium NPs (50 mg/kg) improved various metabolites, including citrate, isocitrate, succinate, malate, 2-oxo-glutarate, and khelmarin D, in lettuce plants to suppress *F. oxysporum* f. sp. *Lactucae*-induced wilt disease [73]. Overall, the influence of multifaceted MnNPs on rhizosphere dynamics highlights their potential as an innovative and sustainable approach to managing Fusarium wilt and other soilborne plant diseases.

Conclusions

This study presents a comprehensive exploration of the antifungal potential of biogenically-synthesized MnNPs against *Fon*, the causative agent of Fusarium wilt in watermelon. MnNPs demonstrated significant antifungal activity by disrupting fundamental biological processes, including hyphal growth, conidiation, and conidial germination, ultimately impairing *Fon* pathogenicity. Transcriptomic analysis revealed that MnNPs induced substantial alterations in gene expression, specifically on the fusaric acid biosynthesis pathway, which plays a critical role in *Fon* virulence. Furthermore, rhizosphere metabolomic profiling highlighted the ability of MnNPs to modulate the soil metabolome, enriching defense-related metabolites and creating an inhibitory environment for *Fon* colonization and infection (Fig. 9). The findings underscore the potential of MnNPs as a novel and effective tool for managing Fusarium wilt in watermelon, offering a sustainable alternative to conventional chemical fungicides. By integrating nanotechnology with agricultural disease management, this study advances our understanding of the molecular and ecological interactions between NPs, pathogens, and plants. Future research should focus on field-scale evaluations and the environmental safety of MnNPs to facilitate their

practical application in sustainable agriculture. Furthermore, future studies should conduct field-scale evaluations to validate the efficacy of MnNPs under diverse environmental conditions and cropping systems. Investigating the mechanisms underlying plant-nanoparticle interactions and optimizing MnNP formulations for controlled release and targeted action will further enhance their applicability.

Supplementary Information

The online version contains supplementary material available at https://doi.org/10.1186/s12951-025-03492-x.

Supplementary Material 1

Acknowledgements
The work is supported by the Zhejiang Key Research and Development Program (Grant no. 2023C02018 and 2022C02047), Zhejiang Provincial Natural Science Foundation (Grant no. LZ20C140001), "Three Agriculture and Nine-organizations" Science and Technology Cooperation Program of Zhejiang Province (Grant no. 2022SNIF012), and the China Postdoctoral Science Foundation (Grant no. 2023M743123 and 2024T170811). The authors would like to extend their sincere appreciation to the Ongoing Research Funding Program (ORF-2025-123), King Saud University, Riyadh, Saudi Arabia. All authors reviewed the manuscript.

Author contributions
Muhammad Noman (Conceptualization, Investigation, Methodology, Formal analysis, Writing-original draft, Validation) Temoor Ahmed (Investigation, Writing - review & editing) Mohammad Shafiqul Islam (Investigation, Formal analysis) Jing Wang (Formal analysis, Writing - review & editing) Yingying Cai (Writing - review & editing) Shuang Liang (Formal analysis) Zhongna Hao (Writing - review & editing) Hayssam M. Ali (Writing - review & editing, Formal analysis) Haiping Qiu (Writing - review & editing) Zhen Zhang (Writing - review & editing) Rongyao Chai (Writing - review & editing) Yanli Wang (Formal analysis, Validation) Bin Li (Formal analysis, Writing - review & editing) Jiaoyu Wang (Funding acquisition, Supervision, Validation, Project administration, Writing - review & editing).

Data availability
No datasets were generated or analysed during the current study.

Declarations

Ethics approval and consent to participate
Not applicable.

Consent for publication
Not applicable.

Competing interests
The authors declare no competing interests.

Author details
[1]State Key Laboratory for Quality and Safety of Agro-Products, Key Laboratory of Agricultural Microbiome of MARA and Zhejiang Province, Key Laboratory of Biotechnology in Plant Protection of MARA and Zhejiang Province, Institute of Plant Protection and Microbiology, Zhejiang Academy of Agricultural Sciences, Hangzhou 310021, China
[2]Xianghu Laboratory, Hangzhou 311231, China
[3]Department of Plant Biotechnology, Korea Universtiy, Seoul 02481, South Korea
[4]State Key Laboratory of Rice Biology and Breeding, Ministry of Agriculture and Rural Affairs Key Laboratory of Molecular Biology of Crop Pathogens and Insect Pests, Zhejiang Key Laboratory of Biology and Ecological Regulation of Crop Pathogens and Insects, Institute of Biotechnology, Zhejiang University, Hangzhou 310058, China
[5]State Key Laboratory for Managing Biotic and Chemical Threats to the Quality and Safety of Agro-Products, Zhejiang Academy of Agricultural Sciences, Hangzhou 310021, China
[6]Department of Botany and Microbiology, College of Science, King Saud University, Riyadh 11451, Saudi Arabia

Received: 23 December 2024 / Accepted: 26 May 2025
Published online: 18 June 2025

References

1. Deng C, Wang Y, Castillo C, Zhao Y, Xu W, Lian J, Rodriguez-Otero K, Brown HJ, Cota-Ruiz K, Elmer WH. Nanoscale iron (Fe_3O_4) surface charge controls fusarium suppression and nutrient accumulation in tomato (*Solanum lycopersicum* L). ACS Sustain Chem Eng. 2024;12:13285–96.
2. Wang Z, Wang T, Wang C, Yue L, Li J, Liu T, Lv Y, White JC, Cao X, Xing B. Lanthanum-based nanomaterials suppress bacterial wilt in tomato: importance of particle morphology and dissolution profiles. Environ Sci Nano. 2023;10:747–60.
3. Ahmed T, Luo J, Noman M, Ijaz M, Wang X, Masood HA, Manzoor N, Wang Y, Li B. Microbe-mediated nanoparticle intervention for the management of plant diseases. Crop Health. 2023;1:3.
4. Varympopi A, Dimopoulou A, Papafotis D, Avramidis P, Sarris I, Karamanidou T, Kerou AK, Vlachou A, Vellis E, Giannopoulos A. Antibacterial activity of copper nanoparticles against *Xanthomonas campestris* pv. *vesicatoria* in tomato plants. Int J Mol Sci. 2022;23:4080.
5. Jian Y, Chen X, Ahmed T, Shang Q, Zhang S, Ma Z, Yin Y. Toxicity and action mechanisms of silver nanoparticles against the mycotoxin-producing fungus *Fusarium graminearum*. J Adv Res. 2021;38:1–12.
6. Shang H, Ma C, Li C, White JC, Polubesova T, Chefetz B, Xing B. Copper sulfide nanoparticles suppress *Gibberella Fujikuroi* infection in rice (*Oryza sativa* L.) by multiple mechanisms: Contact-mortality, nutritional modulation and phytohormone regulation. Environ Sci Nano. 2020;7:2632–43.
7. Shang W, Xiong Q, Xie Z, Cheng J, Yu B, Zhang H, Su Y, Zhao J. Functional, eco-friendly, and starch-based nanocarriers with sustained release of carvacrol for persistent control of tomato Gray mold. Crop Health. 2023;1:13.
8. Guo X, Luo J, Zhang R, Gao H, Peng L, Liang Y, Li T. Root cell wall remodeling mediates copper oxide nanoparticles phytotoxicity on lettuce (*Lactuca sativa* L). Environ Exp Bot. 2022;200:104906.
9. Rutkowski M, Krzemińska-Fiedorowicz L, Khachatryan K, Khachatryan G, Kalisz A, Sękara A. Impact of silver nanoparticles in alginate gels on seed germination, growth and stress biochemical parameters of cucumber seedlings. Plant Stress. 2024;12:100491.
10. Noman M, Ahmed T, Ijaz U, Hameed A, Shahid M, Azizullah, Li D, Song F. Microbe-oriented nanoparticles as phytomedicines for plant health management: an emerging paradigm to achieve global food security. Crit Rev Food Sci Nutr. 2022;63:7489–509.
11. Noman M, Ahmed T, White JC, Nazir MM, Li D, Song F. *Bacillus altitudinis*-stabilized multifarious copper nanoparticles prevent bacterial fruit blotch in watermelon (*Citrullus lanatus* L.): direct pathogen inhibition, *in planta* particles accumulation, and host stomatal immunity modulation. Small. 2023;19:2207136.
12. Noman M, Ahmed T, Ijaz U, Shahid M, Nazir MM, White JC, Li D, Song F. Bio-functionalized manganese nanoparticles suppress Fusarium wilt in watermelon (*Citrullus lanatus* L.) by infection disruption, host defense response potentiation, and soil microbial community modulation. Small. 2023;19:2205687.
13. He S, Chen J, Zhao J, Wang Z, Wu R, Zhang Y. Highly efficient sterilization of biogenic FeS_2 nanoparticles: mechanism and Inhibition of antibiotic resistance. Chem Eng J. 2025;509:160975.
14. Noman M, Ahmed T, Wang J, Ijaz M, Shahid M, Islam MS, Azizullah, Manzoor I, Li D, Song F. Nano-enabled crop resilience against pathogens: potential, mechanisms and strategies. Crop Health. 2023;1:15.
15. Ogunyemi SO, Zhang M, Abdallah Y, Ahmed T, Qiu W, Ali M, Yan C, Yang Y, Chen J, Li B. The bio-synthesis of three metal oxide nanoparticles (ZnO, MnO_2,

and MgO) and their antibacterial activity against the bacterial leaf blight pathogen. Front Microbiol. 2020;11:3099.
16. Perfileva AI, Krutovsky KV. Manganese nanoparticles: synthesis, mechanisms of influence on plant resistance to stress, and prospects for application in agricultural chemistry. J Agric Food Chem. 2024;72:7564–85.
17. Zhang F, Fang M, Hu P, Yao X, Yang C, Lu Z, Wang J, Zhang L. Acidity-activated degradable Mn-engineered silicon nanohybrids coordinated with Iprodione for high-efficiency management of *Sclerotinia sclerotiorum* and nutrient enhancement to crops. Chem Eng J. 2024;486:150265.
18. Lu L, Huang M, Huang Y, Corvini PF-X, Ji R, Zhao L. Mn_3O_4 nanozymes boost endogenous antioxidant metabolites in cucumber *(Cucumis sativus*) plant and enhance resistance to salinity stress. Environ Sci Nano. 2020;7:1692–703.
19. Martyn RD. Fusarium wilt of watermelon: 120 years of research. In *Horticultural Reviews. Volume* 42. Edited by Janick J. New Jersey, USA: Wiley-Blackwell; 2014: 349– 442.
20. Gawehns F, Houterman P, Ichou FA, Michielse C, Hijdra M, Cornelissen B, Rep M, Takken F. The *Fusarium oxysporum* effector Six6 contributes to virulence and suppresses I-2-mediated cell death. Mol Plant-Microb Interact. 2014;27:336–48.
21. López-Díaz C, Rahjoo V, Sulyok M, Ghionna V, Martín-Vicente A, Capilla J, Di Pietro A, López-Berges MS. Fusaric acid contributes to virulence of *Fusarium oxysporum* on plant and mammalian hosts. Mol Plant Pathol. 2018;19:440–53.
22. Gámez-Arjona FM, Vitale S, Voxeur A, Dora S, Müller S, Sancho-Andrés G, Montesinos JC, Di Pietro A, Sánchez-Rodríguez C. Impairment of the cellulose degradation machinery enhances *Fusarium oxysporum* virulence but limits its reproductive fitness. Sci Adv. 2022;8:eabl9734.
23. Chen Q, Liu C, Qi H, Wu N, Liu Z, Tian Q, Zhu X-X, Li X, Chen Y, Ma Z. A novel highly antifungal compound ZJS-178 targeting myosin I inhibits the endocytosis and Mycotoxin biosynthesis of *Fusarium graminearum*. Crop Health. 2024;2:14.
24. Tintor N, Paauw M, Rep M, Takken FL. The root-invading pathogen *Fusarium oxysporum* targets pattern-triggered immunity using both cytoplasmic and apoplastic effectors. New Phytol. 2020;227:1479–92.
25. Li J, Gao M, Gabriel DW, Liang W, Song L. Secretome-wide analysis of lysine acetylation in *Fusarium oxysporum* f. Sp. *lycopersici* provides novel insights into infection-related proteins. Front Microbiol. 2020;11:559440.
26. Noman M, Ahmed T, Shahid M, Nazir MM, Li D, Song F. Salicylic acid-doped iron nano-biostimulants potentiate defense responses and suppress Fusarium wilt in watermelon. J Adv Res. 2023;59:19–33.
27. Mondani L, Chiusa G, Battilani P. Chemical and biological control of *Fusarium* species involved in Garlic dry rot at early crop stages. Eur J Plant Pathol. 2021;160:575–87.
28. Buchman JT, Elmer WH, Ma C, Landy KM, White JC, Haynes CL. Chitosan-coated mesoporous silica nanoparticle treatment of *Citrullus lanatus* (watermelon): enhanced fungal disease suppression and modulated expression of stress-related genes. ACS Sustain Chem Eng. 2019;7:19649–59.
29. Kang H, Elmer W, Shen Y, Zuverza-Mena N, Ma C, Botella P, White JC, Haynes CL. Silica nanoparticle dissolution rate controls the suppression of Fusarium wilt of watermelon (*Citrullus lanatus*). Environ Sci Technol. 2021;55:13513–22.
30. Noman M, Ahmed T, Islam MS, Ahmad M, Wang J, Cai Y, Hao Z, Ali HM, Zhang Z, Wang Y. Antifungal profile and mechanism of bioinspired nanoscale magnesium against the agriculturally important pathogen *Fusarium oxysporum* f. Sp. *niveum*. Environ Sci Nano. 2024;11:4279–92.
31. Adisa IO, Reddy Pullagurala VL, Rawat S, Hernandez-Viezcas JA, Dimkpa CO, Elmer WH, White JC, Peralta-Videa JR, Gardea-Torresdey JL. Role of cerium compounds in Fusarium wilt suppression and growth enhancement in tomato (*Solanum lycopersicum*). J Agric Food Chem. 2018;66:5959–70.
32. Xie X-G, Huang C-Y, Cai Z-D, Chen Y, Dai C-C. Targeted acquisition of *Fusarium oxysporum* f. Sp. *niveum* toxin-deficient mutant and its effects on watermelon Fusarium wilt. J Agric Food Chem. 2019;67:8536–47.
33. Ding Z, Yang L, Wang G, Guo L, Liu L, Wang J, Huang J. Fusaric acid is a virulence factor of *Fusarium oxysporum* f. Sp. *cubense* on banana plantlets. Trop Plant Pathol. 2018;43:297–305.
34. Singh VK, Singh HB, Upadhyay RS. Role of fusaric acid in the development of 'Fusarium wilt' symptoms in tomato: physiological, biochemical and proteomic perspectives. Plant Physiol Biochem. 2017;118:320–32.
35. Phasha M, Wingfield B, Wingfield M, Coetzee M, Hammerbacher A, Steenkamp E. Deciphering the effect of *FUB1* disruption on fusaric acid production and pathogenicity in *Fusarium circinatum*. Fungal Biol. 2021;125:1036–47.
36. Brown DW, Lee S-H, Kim L-H, Ryu J-G, Lee S, Seo Y, Kim YH, Busman M, Yun S-H, Proctor RH. Identification of a 12-gene fusaric acid biosynthetic gene cluster in *Fusarium* species through comparative and functional genomics. Mol Plant-Microb Interact. 2015;28:319–32.
37. Kudjordjie EN, Hooshmand K, Sapkota R, Darbani B, Fomsgaard IS, Nicolaisen M. *Fusarium oxysporum* disrupts microbiome-metabolome networks in *Arabidopsis thaliana* roots. Microbiol Spectr. 2022;10:e01226–01222.
38. Liu Y, Chen L, Wu G, Feng H, Zhang G, Shen Q, Zhang R. Identification of root-secreted compounds involved in the communication between cucumber, the beneficial *Bacillus amyloliquefaciens*, and the soil-borne pathogen *Fusarium oxysporum*. Mol Plant-Microb Interact. 2017;30:53–62.
39. Guo J, Li G, Ijaz M, Hafeez R, Ibrahim E, Ahmed T, Qi X, Zhang S, Ali HM, Li B. Transcriptomic and metabolomic analyses reveal that lignin biosynthesis contributes to bayberry (*Myrica rubra*) defence responses against twig blight. Plant Stress. 2024;13:100514.
40. Zhou X, Zhang J, u Rahman MK, Gao D, Wei Z, Wu F, Dini-Andreote F. Interspecific plant interaction *via* root exudates structures the disease suppressiveness of rhizosphere microbiomes. Mol Plant. 2023;16:849–64.
41. Somasegaran P, Hoben HJ. Handbook for rhizobia: methods in legume-Rhizobium technology. Springer Science & Business Media; 2012.
42. Wiegand I, Hilpert K, Hancock RE. Agar and broth Dilution methods to determine the minimal inhibitory concentration (MIC) of antimicrobial substances. Nat Protoc. 2008;3:163–75.
43. Weisburg WG, Barns SM, Pelletier DA, Lane DJ. *16S* ribosomal DNA amplification for phylogenetic study. J Bacteriol. 1991;173:697–703.
44. Ogier J-C, Pagès S, Galan M, Barret M, Gaudriault S. *rpoB*, a promising marker for analyzing the diversity of bacterial communities by amplicon sequencing. BMC Microbiol. 2019;19:171.
45. Ahmed T, Noman M, Jiang H, Shahid M, Ma C, Wu Z, Nazir MM, Ali MA, White JC, Chen J, Bin L. Bioengineered chitosan-iron nanocomposite controls bacterial leaf blight disease by modulating plant defense response and nutritional status of rice (*Oryza sativa* L). Nano Today. 2022;45:101547.
46. Gao Y, Xiong X, Wang H, Bi Y, Wang J, Yan Y, Li D, Song F. *Fusarium oxysporum* f. Sp. *niveum* pumilio 1 regulates virulence on watermelon through interacting with the ARP2/3 complex and binding to an A-rich motif in the 3' UTR of diverse transcripts. mBio. 2023;14:e00157–00123.
47. Gao Y, Xiong X, Wang H, Wang J, Bi Y, Yan Y, Cao Z, Li D, Song F. Ero1-Pdi1 module-catalysed dimerization of a nucleotide sugar transporter, FonNst2, regulates virulence of *Fusarium oxysporum* on watermelon. Environ Microbiol. 2021;24:1200–20.
48. Azizullah NM, Gao Y, Wang H, Xiong X, Wang J, Li D, Song F. The sumoylation pathway regulates the pathogenicity of *Fusarium oxysporum* f. Sp. *niveum* in watermelon through stabilizing the pH regulator FonPalC *via* sumoylation. Microbiol Res. 2024;281:127632.
49. Kim D, Pertea G, Trapnell C, Pimentel H, Kelley R, Salzberg SL. TopHat2: accurate alignment of transcriptomes in the presence of insertions, deletions and gene fusions. Genome Biol. 2013;14:1–13.
50. Li B, Dewey CN, RSEM. Accurate transcript quantification from RNA-seq data with or without a reference genome. BMC Bioinformatics. 2011;12:1–16.
51. Anders S, Huber W. Differential expression analysis for sequence count data. Nat Preced. 2010:1–1.
52. Young MD, Wakefield MJ, Smyth GK, Oshlack A. Gene ontology analysis for RNA-seq: accounting for selection bias. Genome Biol. 2010;11:1–12.
53. Noman M, Azizullah, Ahmed T, Gao Y, Wang H, Xiong X, Wang J, Lou J, Li D, Song F. Degradation of α-subunits, Doa1 and Doa4, are critical for growth, development, programmed cell death events, stress responses, and pathogenicity in the watermelon Fusarium wilt fungus *Fusarium oxysporum* f. Sp. *niveum*. J Agric Food Chem. 2023;71:11667–79.
54. Zhao L, Zhang H, White JC, Chen X, Li H, Qu X, Ji R. Metabolomics reveals that engineered nanomaterial exposure in soil alters both soil rhizosphere metabolite profiles and maize metabolic pathways. Environ Sci Nano. 2019;6:1716–27.
55. Livak KJ, Schmittgen TD. Analysis of relative gene expression data using real-time quantitative PCR and the $2^{-\Delta\Delta CT}$ method. Methods. 2001;25:402–8.
56. Steel RG, Torrie JH, Dickey DA. Principles and procedures of statistics: A biological approach. New York: McGraw-Hill; 1997.
57. Fujikawa I, Takehara Y, Ota M, Imada K, Sasaki K, Kajihara H, Sakai S, Jogaiah S, Ito S. -i. Magnesium oxide induces immunity against Fusarium wilt by triggering the jasmonic acid signaling pathway in tomato. J Biotech. 2021;325:100–8.
58. Chang T-H, Liu Y-W, Lin Y-H, Lin J-J, Huang J-W, Hussain A, Chang P-FL. Silver nanoparticles on nanoscale silica platelets (AgNP/NSP) and nanoscale silica platelets (NSP) inhibit the development of *Fusarium oxysporum* f. Sp. *niveum*. ACS Appl Bio Mater. 2019;2:4978–85.

59. Deng C, Wang Y, Cantu JM, Valdes C, Navarro G, Cota-Ruiz K, Hernandez-Viezcas JA, Li C, Elmer WH, Dimkpa CO. Soil and foliar exposure of soybean (*Glycine max*) to cu: nanoparticle coating-dependent plant responses. NanoImpact. 2022;26:100406.
60. Dananjaya S, Erandani W, Kim C-H, Nikapitiya C, Lee J, De Zoysa M. Comparative study on antifungal activities of Chitosan nanoparticles and Chitosan silver nano composites against *Fusarium oxysporum* species complex. Int J Biol Macromol. 2017;105:478–88.
61. Gaber SE, Hashem AH, El-Sayyad GS, Attia MS. Antifungal activity of mycosynthesized bimetallic ZnO-CuO nanoparticles against fungal plant pathogen *Fusarium oxysporum*. Biomass Convers Biorefin. 2024;14:25395–409.
62. González-Merino AM, Hernández-Juárez A, Betancourt-Galindo R, Ochoa-Fuentes YM, Valdez-Aguilar LA, Limón-Corona ML. Antifungal activity of zinc oxide nanoparticles in *Fusarium oxysporum-Solanum lycopersicum* pathosystem under controlled conditions. J Phytopathol. 2021;169:533–44.
63. Niehaus E-M, von Bargen KW, Espino JJ, Pfannmüller A, Humpf H-U, Tudzynski B. Characterization of the fusaric acid gene cluster in *Fusarium Fujikuroi*. Appl Microbiol Biotechnol. 2014;98:1749–62.
64. Studt L, Janevska S, Niehaus EM, Burkhardt I, Arndt B, Sieber CM, Humpf HU, Dickschat JS, Tudzynski B. Two separate key enzymes and two pathway-specific transcription factors are involved in fusaric acid biosynthesis in *F Usarium Fujikuroi*. Environ Microbiol. 2016;18:936–56.
65. Portal Gonzalez N, Soler A, Ribadeneira C, Solano J, Portieles R, Herrera Isla L, Companioni B, Borras-Hidalgo O, Santos Bermudez R. Phytotoxic metabolites produce by *Fusarium oxysporum* f. Sp. *cubense* race 2. Front Microbiol. 2021;12:629395.
66. Liu S, Li J, Zhang Y, Liu N, Viljoen A, Mostert D, Zuo C, Hu C, Bi F, Gao H. Fusaric acid instigates the invasion of banana by fusarium oxysporum f. Sp. cubense TR4. New Phytol. 2020;225:913–29.
67. Wen T, Xie P, Liu H, Liu T, Zhao M, Yang S, Niu G, Hale L, Singh BK, Kowalchuk GA. Tapping the rhizosphere metabolites for the prebiotic control of soil-borne bacterial wilt disease. Nat Commun. 2023;14:4497.
68. Yang K, Fu R, Feng H, Jiang G, Finkel O, Sun T, Liu M, Huang B, Li S, Wang X. RIN enhances plant disease resistance *via* root exudate-mediated assembly of disease-suppressive rhizosphere microbiota. Mol Plant. 2023;16:1379–95.
69. Wei C, Liang J, Wang R, Chi L, Wang W, Tan J, Shi H, Song X, Cui Z, Xie Q. Response of bacterial community metabolites to bacterial wilt caused by *Ralstonia solanacearum*: A multi-omics analysis. Front Plant Sci. 2024;14:1339478.
70. Were E, Schöne J, Viljoen A, Rasche F. Phenolics mediate suppression of *Fusarium oxysporum* f. Sp. *cubense* TR4 by legume root exudates. Rhizosphere. 2022;21:100459.
71. Yang K, Zhou G, Chen C, Liu X, Wei L, Zhu F, Liang Z, Chen H. Joint metabolomic and transcriptomic analysis identify unique phenolic acid and flavonoid compounds associated with resistance to Fusarium wilt in cucumber (*Cucumis sativus* L). Front Plant Sci. 2024;15:1447860.
72. Lv J, Dong Y, Dong K, Zhao Q, Yang Z, Chen L. Intercropping with wheat suppressed Fusarium wilt in faba bean and modulated the composition of root exudates. Plant Soil. 2020;448:153–64.
73. Shang H, Ma C, Li C, Cai Z, Shen Y, Han L, Wang C, Tran J, Elmer WH, White JC. Aloe vera extract gel-biosynthesized selenium nanoparticles enhance disease resistance in lettuce by modulating the metabolite profile and bacterial endophytes composition. ACS Nano. 2023;17:13672–84.

Publisher's note